



# A New Butterfly-Inspired Compliant Joint with 3-DOF In-plane Motion

Ngoc Thoai Tran<sup>1</sup> · Ngoc Le Chau<sup>1</sup> · Thanh-Phong Dao<sup>2,3</sup>

Received: 17 August 2019 / Accepted: 12 February 2020 / Published online: 26 February 2020  
© King Fahd University of Petroleum & Minerals 2020

## Abstract

This paper proposes a new butterfly-inspired compliant joint by combining a butterfly's profile and a foldable mechanism. The joint can achieve three degrees of freedom in its fabrication plane, including two translations in the  $x$ - and  $y$ -axes and a rotary motion around the  $z$ -axis. Equivalent spring stiffness of the joint is easy to be adjusted by adopting a foldable mechanism, while a butterfly's profile gives better compliance. Closed-form model of the joint is established to calculate stiffness, displacement, and rotational angle. Performances and effectiveness of the proposed joint are verified by comparing with other joints. A prototype is fabricated, and experiments are conducted. The results show a good agreement between the analytical model, simulation, and experiment. Compared with a conventional rectangular flexure joint in terms of bending displacement and compressive displacement, the results found that performances of the joint are greatly improved. Bending displacement and angular displacement of the joint are increased by up to 14.6% and 12.6%, respectively. The proposed joint can be considered as a potential candidate for a precise positioning system.

**Keywords** Compliant joint · Compliant mechanism · Closed-form model · Finite element analysis

## 1 Introduction

A compliant joint is a basic element of compliant mechanism which is utilized to transfer force, torque, motion, or energy [1, 2]. Compliant mechanism has emerging properties, e.g., free friction, no lubricant, reduced assembly, and low manufacturing cost. It can be monolithically fabricated by emerging techniques such as wire electrical discharge machining or 3D, 4D printing, or CNC machining. Nowadays, compliant joints have been fast grown for use in ultrahigh-precision instruments [3], tissue cutting [4], and microelectronic devices [5–7], and vibration suspension [8]. It is noted that the shape and number of degrees of freedom (DOF) of a compliant joint are two common characteristics that have been received great interest. The reasons are that if

the shape or number of DOFs is well designed, performances of a joint can be improved accordingly.

In order to meet various positioning tasks, a lot of different shapes for compliant joint, called as flexure hinge, were proposed, e.g., right circular flexure hinge [9], elliptical-arc flexure hinges [10], damped leaf hinge [11], and parabolic flexure hinge [12]. For biomechanical rehabilitation and assistive technology, rotary compliant joints were created thanks to their simple structure, lightweight, and low manufacturing cost [13, 14]. Moreover, a good compliant behavior can be made by changing the thickness of a compliant joint but this may cause a positioning error and undesired oscillation [15]. In overcome this circumstance, a circular hinge was integrated with a damper so as to harvest outside vibrations [16]. On the other hand, the shape of a compliant joint can be adjusted according to designer's experience or customer. However, the number of DOFs of a compliant joint has been facing challenges for researchers. A new compliant joint with multiple DOFs is motivated in the present paper.

Regarding the number of DOFs of a joint, existing compliant joints have been created for 1-DOF positioning mechanisms and suppressed other DOFs. There have been some efforts on designing a hybrid flexure with bidirectional motion, e.g., a power-function-shaped flexure hinge [17], hybrid bidirectional flexure joint [18], right circular

✉ Thanh-Phong Dao  
daothanhpung@tdtu.edu.vn

<sup>1</sup> Faculty of Mechanical Engineering, Industrial University of Ho Chi Minh City, Ho Chi Minh City, Vietnam

<sup>2</sup> Division of Computational Mechatronics, Institute for Computational Science, Ton Duc Thang University, Ho Chi Minh City, Vietnam

<sup>3</sup> Faculty of Electrical and Electronics Engineering, Ton Duc Thang University, Ho Chi Minh City, Vietnam



hinge, elliptical-arc, parabolic, and hyperbolic shapes [19]. In order to improve the flexibility of joint, a straight-axis flexure hinge was designed [20] and a flexure hinge with multi-cavity was suggested [21]. Besides, many different configurations of a joint were developed, such as a triple-cross-spring flexure joint [3], a serial flexure [22], a flexure hinge with a variable cross section [23], and flexure arrays [24]. In addition, researchers suggested emerging joints, e.g., cross-axis-flexural pivot [25], large-displacement compliant [26], flexure hinge with topology optimization [27], deep-notch elliptical flexure hinge [28], leaf flexure hinge [29], tape-spring hinge [30], hybrid non-symmetric flexure hinge [31], flexure hinge with large displacement [32], cracked right circular flexure hinge [9], flexure magnifying mechanism [33], and a flexure hinge for sensing device [34]. Recently, a compliant joint with a thin wall was designed for camera device [35, 36] and flexural joint with Q shape was proposed so as to enhance the deflection of joint [37].

Although previous studies have been well developed many different types of compliant joints, they almost focused on designing shapes. Up to now, a compliant joint with multiple DOFs is a lack of interest. In order to fulfill this requirement, the present study proposes a new compliant joint by a combination of a foldable mechanism and a butterfly's profile. A foldable mechanism is adopted to adjust the stiffness of the joint. The stiffness is proportional to the deflection of the compliant joint; therefore, if the stiffness is varied, the deflection is changed accordingly [38]. Meanwhile, observed from the nature, the butterfly's profile is very flexible based on its wings. So, the proposed joint can mimic the butterfly's profile to make a good compliance. In this study, a new joint is named as a new butterfly-inspired compliant joint (BICJ) which is a combination of mechanical structure and nature animal. The main contributions of this article are as follows: (i) The proposed BICJ permits three DOFs in its fabricating plane, including 1-DOF translation in the  $x$ -axis, 1-DOF translation in the  $y$ -axis, and 1-DOF rotary motion around the  $z$ -axis. (ii) The proposed BICJ reaches multiple good performances in terms of bending displacement, compressive displacement, and angular displacement.

The goals of this article are to design and analyze a new compliant joint. The proposed BICJ joint is inspired by a butterfly's profile and a foldable mechanism. It is capable of allowing multiple flexibilities in three directions. Performances of the proposed BICJ are compared with other joints by using numerical analysis. A closed-form model of the joint is derived so as to calculate the stiffness, displacement, and rotation angle. Simulation and experiments are performed to verify the analytical model.

## 2 Conceptual Design

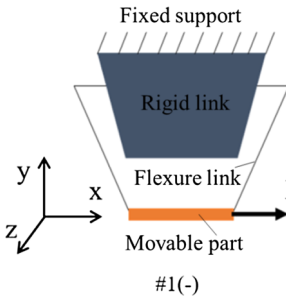
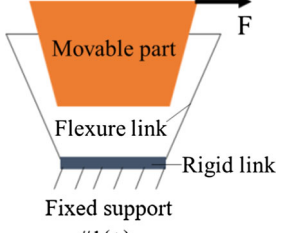
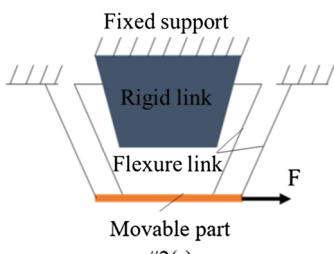
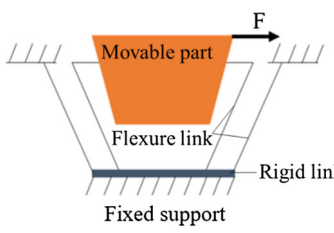
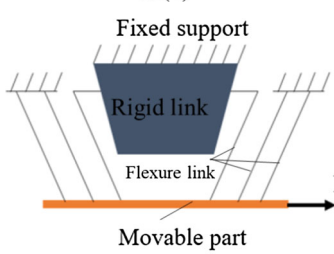
As mentioned above, the aim of this article is to create a new compliant joint, BICJ, in terms of 1-DOF motion in the  $x$ -axis, 1-DOF motion in the  $y$ -axis, and 1-DOF rotary motion around the  $z$ -axis. In addition, the proposed BICJ has a large range of load being suitable for different applications, and its stress concentration is smaller than the yield strength of the material to ensure a good enough working strength. Before creating the BICJ, it begins with a common compliant joint where a free rigid end, a flexure body, and a fixed end are composed together. This section gives a conceptual design to form a new joint, and the kinematic diagram of different configurations of a joint is analyzed. Various configurations of joints are classified, as shown in Table 1.

Table 1 gives eight single configurations of a compliant joint. A fixed rigid link is labeled with gray color, a movable rigid link is labeled with orange color, and a flexure body is the thinnest link. Configuration #1(–) includes two leaf hinges, a movable part and a fixed part. Signal #1(–) shows a load at the bottom part. Configuration #1(+) notes that a load is at the top part. Both these two configurations can subject a very small load. They can make a small rotation angle, small bending displacement, and very small stiffness. Next, both configurations #2(–) and #2(+) are assigned by adopting four flexures, three fixed parts, and a movable element. Both these two configurations give a small capacity of load, small rotational angle, small bending displacement, and small stiffness. Both configurations can only achieve 1-DOF motion but limit multiple DOFs.

Next, configurations #3(–) and #3(+) are designed by using six flexures, three fixed parts, and a movable element. Both these configurations permit a middle load, middle rotational angle, middle displacement, and middle stiffness. Subsequently, configurations #4(–) and #4(+) are assigned via adopting six flexures, three fixed parts, and a movable element. Both these configurations make a relatively large load, large rotational angle, large bending displacement, and large stiffness.

In order to develop a new BICJ with three DOFs, a concept of a compound joint is introduced herein. According to previous studies [15, 38–40], if the length of the flexure hinge is enlarged, the displacement is increased. From this point of view, a combination of single configurations in Table 1 is suggested to create a compound configuration. Table 2 gives seven different compound configurations. By combining configurations #1(–) and #1(+), a first compound configuration #11 is made with four-leaf hinges, a movable part, and a fixed part. Configuration #11 has some characteristics such as very small load, very large rotational angle, very large bending displacement, and very small stiffness. Next, configuration #2(–) is coupled with configuration #2(+) to make a configuration #22 consisting of 8 leaf hinges, a mov-

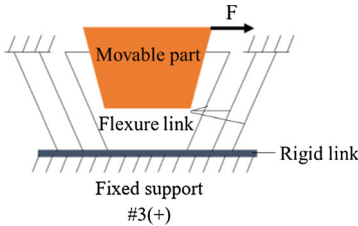
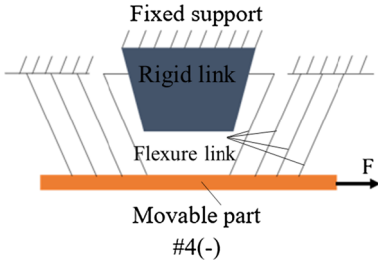
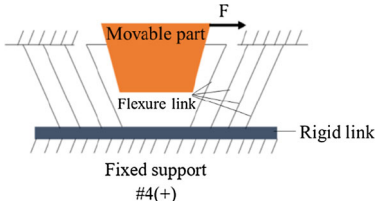
**Table 1** Single configurations of a compliant joint

No.	Type of configuration	Boundary condition	Specification
1	 <p>#1(-)</p>	02 Leaf hinges 01 Movable part 01 Fixed part	Very small capacity of load Very small rotational angle Small bending displacement Very small stiffness 1-DOF in-plane motion
2	 <p>#1(+)</p>	02 Leaf hinges 01 Movable part 01 Fixed part	Very small capacity of load Very small rotational angle Small bending displacement Very small stiffness 1-DOF in-plane motion
3	 <p>#2(-)</p>	04 Leaf hinges 01 Movable part 03 Fixed parts	Small capacity of load Small rotational angle Small bending displacement Small stiffness 1-DOF in-plane motion
4	 <p>#2(+)</p>	04 Leaf hinges 01 Movable part 03 Fixed parts	Small capacity of load Small rotational angle Small bending displacement Small stiffness 1-DOF in-plane motion
5	 <p>#3(-)</p>	06 Leaf hinges 01 Movable part 03 Fixed parts	Middle capacity of load Middle rotational angle Middle displacement Middle stiffness 1-DOF in-plane motion

able part, and 5 fixed part. Characteristics of configuration #22 include a small load, small rotational angle, small bending displacement, and low stiffness. Configuration #33 is a combination of #3(-) and #3(+), that is composed of 12 leaf hinges, a movable part, and 5 fixed parts. This configuration allows a small load, small rotational angle, small bending

displacement, and small stiffness. Configuration #44 is constructed by combining the configuration #4(-) and #4(+). It consists of 16 leaf hinges, a movable part, and 5 fixed parts. Its characteristics include a small load, small rotational angle, small bending displacement, and small stiffness. Besides, configuration #X is a common configuration consisting of 4

Table 1 continued

No.	Type of configuration	Boundary condition	Specification
6	 <p>Movable part Flexure link Rigid link Fixed support #3(+)</p>	06 Leaf hinges 01 Movable part 03 Fixed parts	Middle capacity of load Middle rotational angle Middle displacement Middle stiffness 1-DOF in-plane motion
7	 <p>Fixed support Rigid link Flexure link Movable part #4(-)</p>	08 Leaf hinges 01 Movable part 03 Fixed parts	Relative large capacity of load Relative large rotational angle Relative large bending displacement Relative large stiffness 1-DOF in-plane motion
8	 <p>Movable part Flexure link Rigid link Fixed support #4(+)</p>	08 Leaf hinges 01 Movable part 03 Fixed parts	Relative large capacity of load Relative large rotational angle Relative large bending displacement Relative large stiffness 1-DOF in-plane motion

(-) Load acts at bottom part

(+) Load acts at top part

leaf hinges, a movable part, and a fixed part. This configuration allows a very small load, very large rotational angle, very large bending displacement, and very small stiffness.

In comparison with existing configurations, this paper proposes two different configurations of the BICJ joint, as shown in Fig. 1a and b. The first configuration is labeled as #half BICJ that has 8 leaf hinges, a movable part, and a fixed part. Its characteristics include a middle load, middle rotational angle, middle bending displacement, and middle stiffness. Another configuration is labeled as #full BICJ, called as a proposed BICJ, with four wings that inspired from a butterfly's profile. This configuration includes 16 leaf hinges, a movable part, and a fixed part. It permits a very large load, large rotational angle, large bending displacement, and very small stiffness. It is assumed that the performances of proposed BICJ are better than other configurations.

The dimensional diagram of the proposed BICJ is provided in Fig. 2 and Table 3. In this study, a foldable mechanism is coupled with the butterfly's profile to create the proposed BICJ. As depicted in Fig. 2, the flexibility of the proposed BICJ is strongly dependent on four springs with stiffness  $k_1$ ,  $k_2$ ,  $k_3$ , and  $k_4$ . It is noted that a compliant joint is easy to flexible and sensitive to oscillation. Thus, the second and third beams of BICJ are utilized to guarantee a good enough stiffness during the joint's working opera-

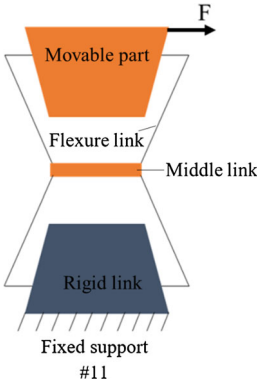
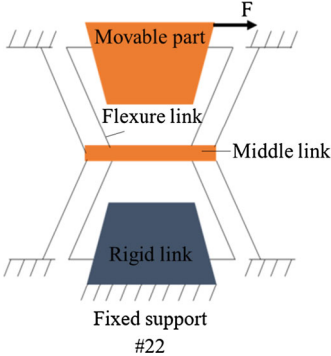
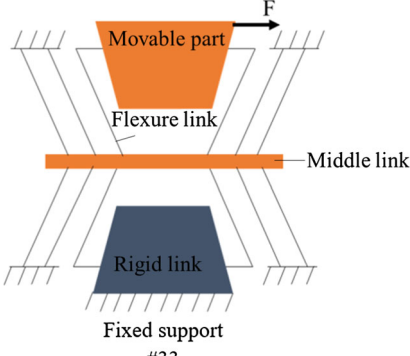
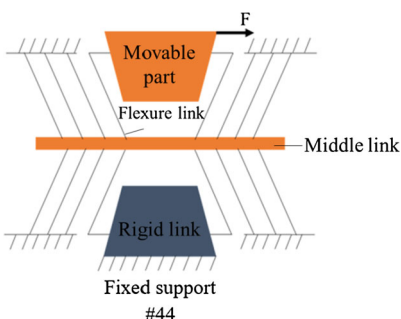
tion. Emerging performances of BICJ include axial motion, and bending motion, and rotary motion. The configuration #full BICJ is chosen for analyzing in this study because it can achieve 3-DOFs in three axes. The proposed BICJ is a potential candidate for multiple functions in positioning engineering. Performances and effectiveness of the proposed BICJ are proved in a later section by comparing with other configurations.

### 3 Comparison of Compound Configurations

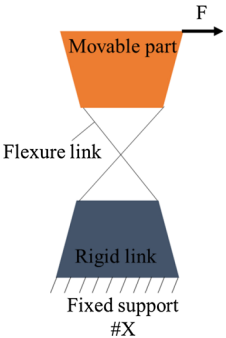
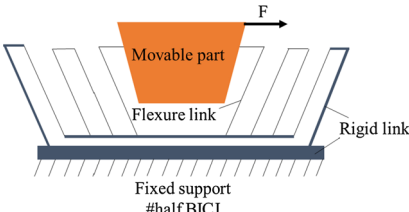
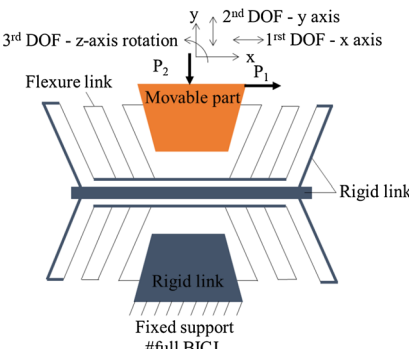
In this section, the performances and effectiveness of the proposed BICJ are validated through a comparison with both configurations #33 and #X. Three configurations, #33 and #X, and # BICJ have the same dimensions. A finite element analysis (FEA) in ANSYS 18.1 software is implemented for this comparison. 3D models of three configurations are constructed in Solidworks 2018 and then imported into ANSYS. Al T73-7075 material is used because of its high yield strength and light density. The mechanical properties are given in Table 4.

The boundary conditions and loads for three configurations (#33, #X, and #BICJ) are shown in Fig. 3. The tetrahedron method is utilized for meshing. Ten-node tetra-

**Table 2** Compound configurations of a compliant joint

No.	Type of configuration	Boundary condition	Specification
1	 <p>#11</p>	<p>04 Leaf hinges 01 Movable part 01 Fixed part</p>	<p>Very small capacity of load Very large rotational angle Very large bending displacement Very small stiffness 1-DOF in-plane motion</p>
2	 <p>#22</p>	<p>08 Leaf hinges 01 Movable part 05 Fixed part</p>	<p>Small capacity of load Small rotational angle Small bending displacement Low stiffness 1-DOF in-plane motion</p>
3	 <p>#33</p>	<p>12 Leaf hinges 01 Movable part 05 Fixed parts</p>	<p>Small capacity of load Small rotational angle Small bending displacement Small stiffness 1-DOF in-plane motion</p>
4	 <p>#44</p>	<p>16 Leaf hinges 01 Movable part 05 Fixed parts</p>	<p>Small capacity of load Small rotational angle Small bending displacement Small stiffness 1-DOF in-plane motion</p>

**Table 2** continued

No.	Type of configuration	Boundary condition	Specification
5		04 Leaf hinges 01 Movable part 01 Fixed part	Very small capacity of load Very large rotational angle Very large bending displacement Very small stiffness 1-DOF in-plane motion
6		08 Leaf hinges 01 Movable part 01 Fixed part	Middle capacity of load Middle rotational angle Middle bending displacement Middle stiffness 1-DOF in-plane motion
7		16 Leaf hinges 01 Movable part 01 Fixed part	Very large capacity of load Large rotational angle Large bending displacement Small stiffness 3-DOF in-plane motion (2-DOF in x- and y-axes and 1-DOF rotation about z-axis)

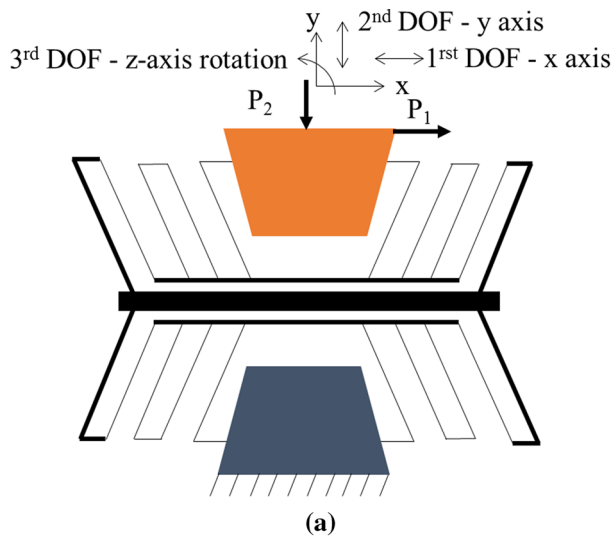


**Fig. 1** Model of the joint: **a** configuration # BICJ, **b** butterfly's profile



**Fig. 2** Dimensions of proposed BICJ joint

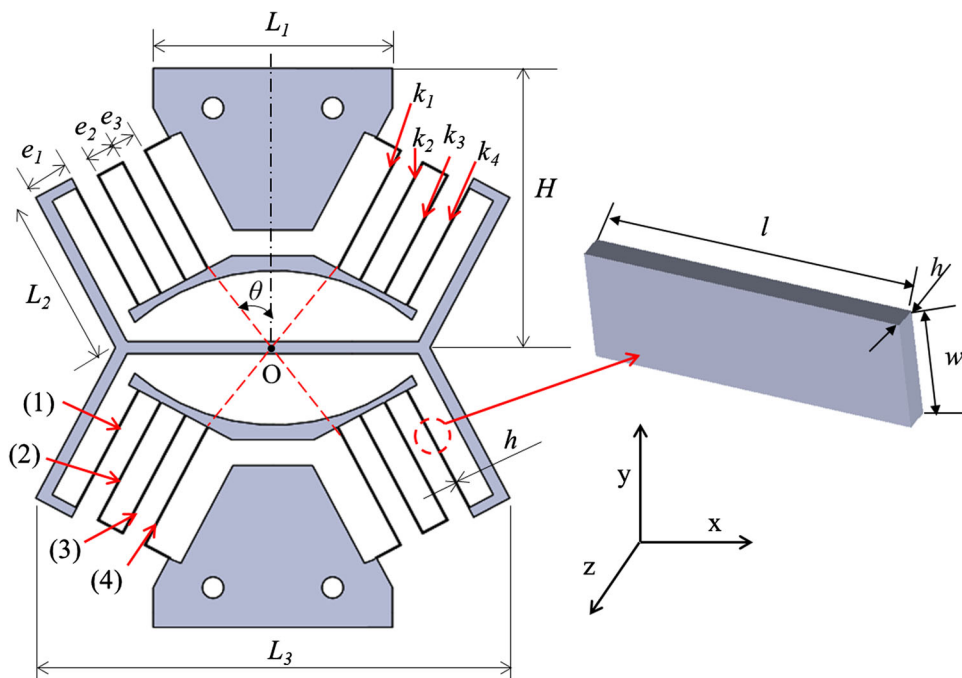


**Table 3** Dimension of the proposed BICJ joint

Dimension	$L_1$ (mm)	$L_2$ (mm)	$L_3$ (mm)	$e_1$ (mm)	$e_2$ (mm)	$e_3$ (mm)	$\theta$ (°)	$H$ (mm)	$h$ (mm)	$l$ (mm)	$w$ (mm)
Value	90	64	178	15	11	10	39	102	0.5	50	10

**Table 4** Mechanical properties of Al T73-7075

Young's modulus (MPa)	Yield strength (MPa)	Poisson ratio	Density ( $\text{kg/m}^3$ )
71,700	503	0.333	2770

hedral element, SOLID92 element configuration, is adopted in this analysis. The meshes of flexure hinges are refined to

achieve accurate results. The meshing models of three configurations are given, as in Fig. 4. A meshing refinement for proposed BICJ is presented, as in Fig. 5. Configuration #33 includes a number of nodes of 61,569 and a number of elements of 27,851. For #X configuration, the number of nodes is 15,736 and the number of elements is 7165. For the proposed BICJ, the number of nodes is 47,176 and the number of elements is 21,040. Meshing quality for the proposed BICJ is evaluated by using skewness criteria and its average

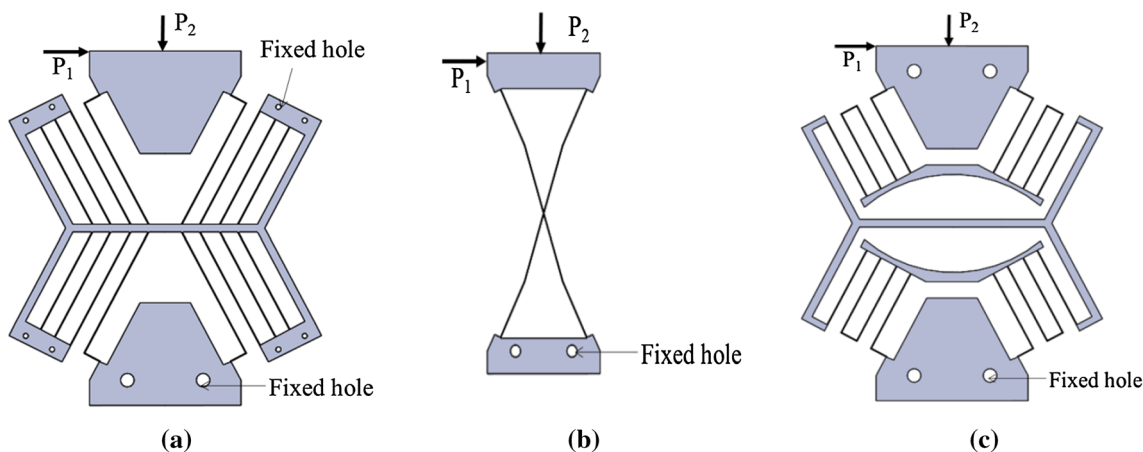


**Fig. 3** Three configurations: a #33, b #X, and c #full BICJ

**Fig. 4** Meshing model of three configurations: **a** #33, **b** #X, and **c** #full BICJ

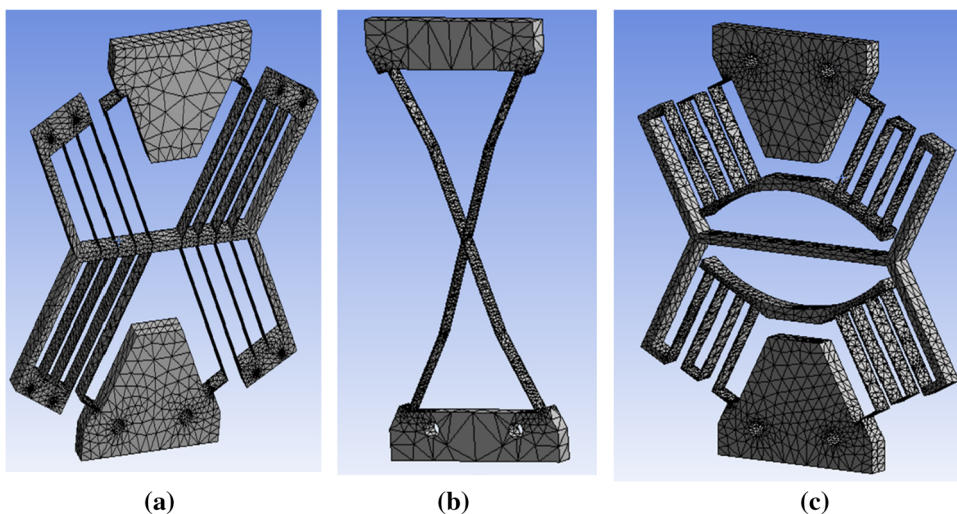


**Fig. 5** Meshing refinement of proposed BICJ joint

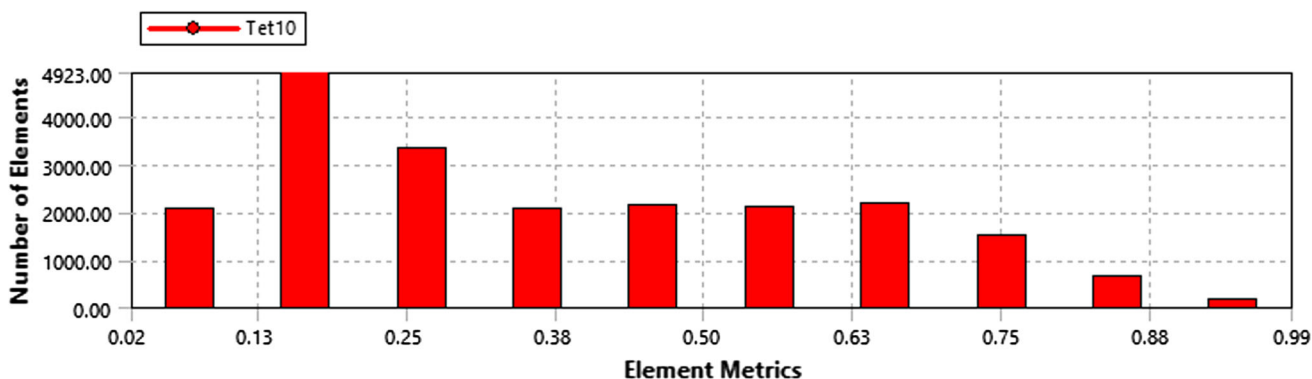
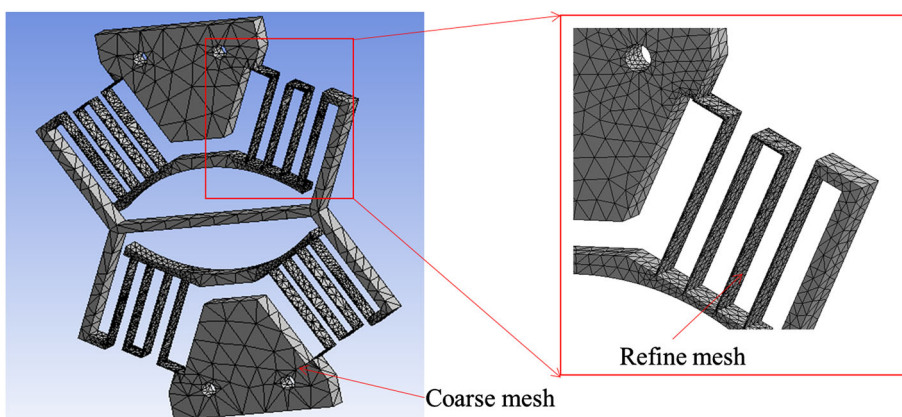


**Fig. 6** Distribution of skewness criteria for the proposed BICJ joint

value is about 0.35, as shown in Fig. 6. This value guarantees an accurate analysis. Moreover, a meshing convergence is investigated on the proposed BICJ to reach a more accurate solution. To study the convergence of the mesh model, a force  $P_1$  of 4 N is exerted on the BICJ, and then a convergent curve of the stress versus the number of elements is plotted, as given in Fig. 7. It found that the meshing model is converged at the elements of 21,040.

### 3.1 Analysis of Bending Displacement

Bending displacement of the proposed BICJ in the  $x$ -axis is the first specification. By using FEA simulation, a load  $P_1$  with the value from 2 to 14 N is exerted to a free end, as given in Fig. 3. The results of Table 5 show that the displacement of configuration #X joint is highest, followed by configuration #33, and configuration # BICJ is lowest. Also, the von



**Fig. 7** Meshing convergence of the proposed BICJ joint

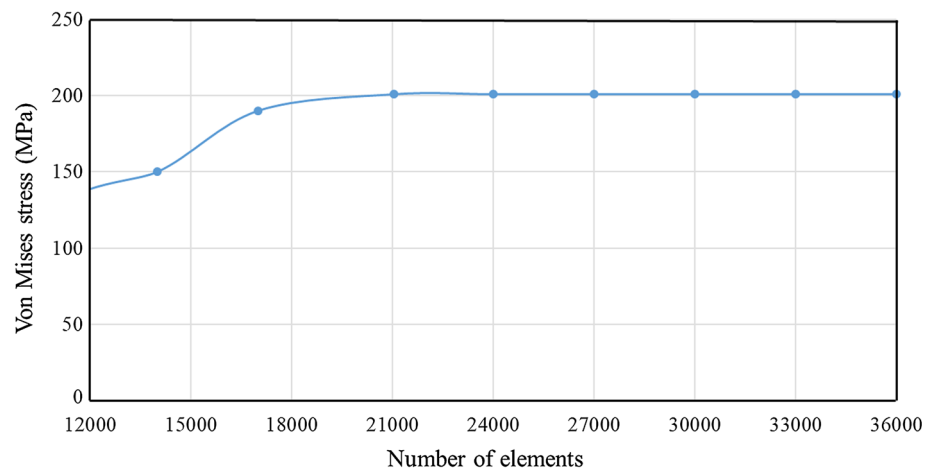


**Table 5** Bending displacement: #33 joint, #X joint, and #full BICJ

$P_1$ (N)	2	4	6	8	10	12	14
<b>#33 Joint</b>							
Displacement (mm)	19.742	39.484	59.226	79.968	98.71	118.5	138.19
Stress (MPa)	188.97	377.93	566.9	755.87	944.84	1133.8	1322.8
<b>#X joint</b>							
Displacement (mm)	68.809	137.62	206.43	275.24	344.05	412.86	481.66
Stress (MPa)	255.56	511.11	766.67	1022.2	1277.8	1533.3	1788.9
<b>#full BICJ</b>							
Displacement (mm)	8.1533	16.307	24.46	32.613	40.766	48.92	57.073
Stress (MPa)	100.38	200.75	301.13	401.51	501.88	602.26	702.64

Mises stress equivalent stress of configuration #X is highest, followed by configuration #33, and configuration # BICJ is smallest.

Besides, the resulting stress of #33 joint is larger than that of yield strength of proposed material at the load  $P_1$  of 6 N. It notes that the #33 joint has a static failure if the load is over 6 N. Considering the #X joint, the strength limitation of this joint is less than 4 N. Meanwhile, the proposed BICJ can work in a wide range of load from 2 to 10 N without static failures. Therefore, the proposed BICJ is more effective than other configurations and it can be promising candidate for use in positioning applications.

### 3.2 Analysis of Compressive Displacement

For a vibration isolator or energy harvester, a compressive displacement of the proposed BICJ in the y-axis is the second specification which is used to suppress vibrations. To conduct this analysis, a load  $P_2$  from 2 to 14 N is used to act to a free end of three mentioned configurations (#33, #X, and #BICJ). Boundary conditions are assigned, as depicted in Fig. 3. Simulation results for three configurations are recorded in Table 6. The results find that the compressive displacement of proposed BICJ is largest, followed by con-

figuration #33, and configuration #X. Besides, the von Mises equivalent stress of three configurations is still under the yield strength of proposed material. This permits a safety working condition. Regarding a large displacement, the proposed BICJ is expected to be an appropriate candidate for future applications.

### 3.3 Analysis of Buckling Deformation

In addition to the compressive displacement, buckling phenomenon is considered for a vibration harvester. It determines the critical buckling load or called safe factor before buckling phenomenon is occurred. This phenomenon may be an error of an engineering structure but it benefits of flexible structure, a flexible spring, to harvest vibrations for a vibration harvester. Assume that configurations #33, #X, and proposed #BICJ are considered as cantilever column. The critical buckling load,  $P_c$ , is as follows [22]:

$$P_c = \frac{EI\pi^2}{4L^2}, \tag{1}$$

**Table 6** Compressive displacement: #33 joint, # X joint, and #full BICJ

$P_2$ (N)	2	4	6	8	10	12	14
<b>#33 joint</b>							
Displacement ( $\times 10^{-5}$ mm)	1.049	2.099	3.132	4.177	5.211	6.265	7.309
Stress (MPa)	19.29	38.58	58.812	75.749	94.687	113.62	132.56
<b>#X joint</b>							
Displacement (mm)	0.010	0.020	0.030	0.040	0.050	0.060	0.070
Stress (MPa)	3.51	7.02	10.54	14.05	17.57	21.08	24.59
<b>#full BICJ</b>							
Displacement ( $\times 10^{-5}$ mm)	5.298	10.597	15.89	21.194	26.493	31.791	37.09
Stress (MPa)	17.62	35.25	52.88	70.50	88.13	105.76	123.39

**Table 7** Buckling under load  $P_1$ : #33 joint, #X joint, and #full BICJ

Load	$P_1$ (N)						
Multiplier load	2	4	6	8	10	12	14
<b>#33 joint</b>							
$\lambda$ of mode 1	-32.678	-16.339	-10.892	-8.1694	-6.5349	-5.4453	-4.6675
$\lambda$ of mode 2	15.091	7.5669	5.0602	3.7834	3.0083	2.5281	2.1635
<b>#X joint</b>							
$\lambda$ of mode 1	-4.6545	-2.3273	-1.5567	-1.1621	-0.92951	-0.7757	-0.6639
$\lambda$ of mode 2	4.8058	2.4029	1.6019	1.2014	0.9612	0.8009	0.6865
<b>#full BICJ</b>							
$\lambda$ of mode 1	-24.429	-12.214	-8.1428	-6.1069	-4.8856	-4.071	-3.489
$\lambda$ of mode 2	20.907	10.458	6.9729	5.2289	4.1846	3.4865	2.988

where  $E$  is Young's modulus,  $I$  is second moment of area, and  $L$  is length of a joint. A simplified equation for the critical buckling load is described by

$$P_c = \lambda \times P_l, \quad (2)$$

where  $\lambda$  is eigenvalue or multiplier load.

Loads  $P_1$  and  $P_2$  from 2 to 14 N are acted to three configurations along the  $x$ - and  $y$ -axes, respectively. By using FEA simulation, the multiplier load,  $\lambda$ , is retrieved in Table 7. Under load  $P_1$ , the results reveal that multiplier load for both modes 1 and 2 of configuration X is highest, followed the BICJ, and configuration #33. With load  $P_2$ , the multiplier load of the BICJ is largest, followed by configuration #33, and configuration #X, as given in Table 8. This specification of BICJ can be promising specification for a vibration harvester.

### 3.4 Analysis of Rotational Angle

Rotational angle of the BICJ is the third specification where the proposed joint may be utilized for a rotary platform. By using load  $P_1$  from 2 to 14 N and boundary conditions in Fig. 3, the simulation results are recorded in Table 9. It determines that the rotation angle of proposed BICJ is from  $3^\circ$  to  $18^\circ$ . The proposed BICJ can withstand a maximum load

of 10 N without static failure. Meanwhile, configuration #33 can rotate an angle from  $9^\circ$  to  $18^\circ$  but it only be used at maximum load of 4 N without static failure. Besides, configuration #X only rotates an angle of  $37^\circ$  and other cases are failed. Considering a capacity of load with a large bending angle, the proposed BICJ is preferred for positioning systems.

## 4 Closed-Form Model of Proposed BICJ Joint

When the proposed BICJ is subjected to a load, elastic energy is stored inside the structure of joint. Therefore, force–displacement curve is critically important to discover the BICJ's characteristics. The relation of force and displacement can be formulated by adopting the joint is simplified as a spring system, and all individual spring constants are combined into a single equivalent spring constant. In this article, the proposed BICJ consists of four significant springs with their stiffnesses labeled as  $k_1$ ,  $k_2$ ,  $k_3$ ,  $k_4$ , as shown in Fig. 2. These springs are arranged in a parallel and series system, as illustrated in Fig. 8.

According to the Euler–Bernoulli beam theory, bending stiffness of beam is calculated by

$$k = \frac{3EI}{l^3} \quad (3)$$

**Table 8** Buckling under load  $P_2$ : #33 joint, #X joint, and #full BICJ

Load	$P_2$ (N)						
	Multiplier load	2	4	6	8	10	12
<b>#33 joint</b>							
$\lambda$ of mode 1	4.0539	2.027	1.3503	1.0127	0.81016	0.67513	0.57869
$\lambda$ of mode 2	34.078	17.039	11.357	8.5177	6.8141	5.6784	4.8672
<b>#X joint</b>							
$\lambda$ of mode 1	1.5096	0.7548	0.50333	0.37743	0.30199	0.2516	0.2157
$\lambda$ of mode 2	17.836	8.9181	5.9455	4.4591	3.5672	2.9729	2.5481
<b>#full BICJ</b>							
$\lambda$ of mode 1	8.6702	4.3351	2.8903	2.1677	1.7341	1.4451	1.2386
$\lambda$ of mode 2	9.0358	4.5179	3.0119	2.2589	1.8071	1.5059	1.2908

**Table 9** Bending angles: #33 joint, #X joint, and #full BICJ

	$P_1$ (N)	2	4	6	8	10	12	14
<b>#33 joint</b>								
Angle (°)	9.059	18.118	27.177	36.236	45.295	54.354	63.413	
Stress (MPa)	188.97	377.93	566.9	755.87	944.84	1133.8	1322.8	
<b>#X joint</b>								
Angle (°)	37.053	74.107	111.16	148.21	185.27	222.32	259.37	
Stress (MPa)	255.56	511.11	766.67	1022.2	1277.8	1533.3	1788.9	
<b>#full BICJ</b>								
Angle (°)	3.608	7.216	10.825	14.433	18.041	21.649	25.258	
Stress (MPa)	100.38	200.75	301.13	401.51	501.88	602.26	702.64	

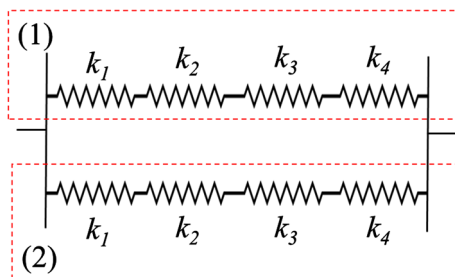


**Fig. 8** Equivalent spring system

where  $k$  is stiffness or spring constant,  $E$  is Young’s modulus,  $I$  is beam’s moment of inertia, and  $l$  is the length of beam.

Beam’s moment of inertia is accounted as

$$I = \frac{bh^3}{12} \tag{4}$$

where  $b$  and  $h$  are width and thickness of beam, respectively.

From the relation of force, stiffness, and deflection, the displacement of bending of beam is computed by

$$\delta = \frac{P}{k} \tag{5}$$

where  $\delta$ ,  $P$ , and  $k$  are the displacement, load, and stiffness, respectively.

According to the relation of springs in Fig. 8, the spring system 1 includes  $k_1, k_2, k_3,$  and  $k_4$  in parallel and series. So, the general form of equivalent stiffness of spring system 1 is found as

$$\frac{1}{k_{eq1}} = \frac{1}{k_1} + \frac{1}{k_2} + \frac{1}{k_3} + \frac{1}{k_4} = \frac{4}{k} \tag{6}$$

where  $k_{eq1}$  is the equivalent stiffness of spring system 1 and  $k_1, k_2, k_3,$  and  $k_4$  are stiffness of flexure hinge 1, 2, 3, and 4 respectively.

Equation (6) is simplified by

$$k_{eq1} = \frac{k}{4} \tag{7}$$

As shown in Fig. 8, the spring system 2 is similar to the spring system 1, and the equivalent stiffness of system 2 is equal to the one of system 1 as follows:

$$k_{eq2} = k_{eq1} = \frac{k}{4} \tag{8}$$

where  $k_{eq2}$  is the equivalent stiffness of spring system.

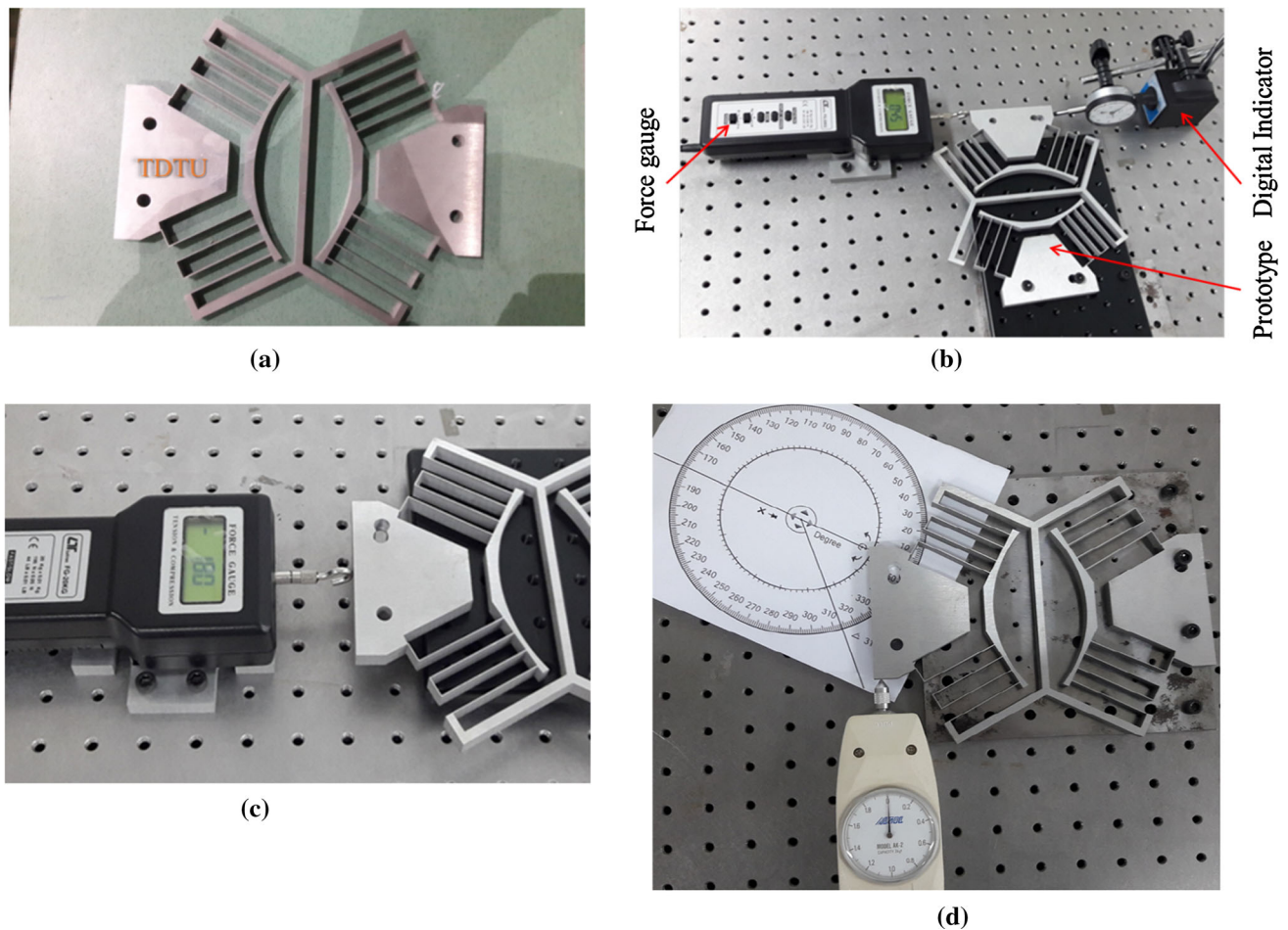


**Fig. 9** Experimental photos: **a** prototype, **b** bending, **c** compress, **d** angle

Because both spring systems 1 and 2 are parallel each other, the equivalent stiffness of entire system is calculated by

$$k_{eq} = k_{eq1} + k_{eq2} = \frac{k}{2} \quad (9)$$

where  $k_{eq}$  is total stiffness of entire system.

In order to evaluate an improvement of performances of the proposed BICJ, the proposed BICJ's characteristics are compared with the ones of the rectangular flexure joint.

An increase in bending displacement is determined as

$$I_b = \left| \frac{\delta_x - \text{BICJ} - \delta_x - \text{flexure}}{\delta_x - \text{flexure}} \right| \times 100 \quad (10)$$

where  $I_b$  represents an increase in bending displacement.  $\delta_x - \text{BICJ}$  and  $\delta_x - \text{flexure}$  are the bending displacements in the  $x$ -axis of the proposed BICJ and rectangular flexure joint.

An increase in angular displacement is determined as

$$I_a = \left| \frac{\theta_{\text{BICJ}} - \phi_{\text{flexure}}}{\phi_{\text{flexure}}} \right| \times 100 \quad (11)$$

where  $I_a$  represents an increase in angular displacement or rotation angle.  $\theta_{y-\text{BICJ}}$  and  $\theta_{\text{flexure}}$  are rotation angle of the proposed BICJ and rectangular flexure joint, respectively.

The relation of moment and bending angle is

$$\theta = \frac{M}{k_{eq}} \quad (12)$$

where  $\theta$  is rotation angle of the joint in degree,  $M$  is moment load in N mm.

## 5 Experimental Investigations

### 5.1 Performance Evaluations

The experimental investigations are established to realize the BICJ's performances and validate the analytical models. Al T73-7075 material was used to fabricate the prototype of the proposed joint, as shown in Fig. 9a. The prototype was mounted on a base fixed to the vibration isolation system table to suppress any vibrations. In order to measure the

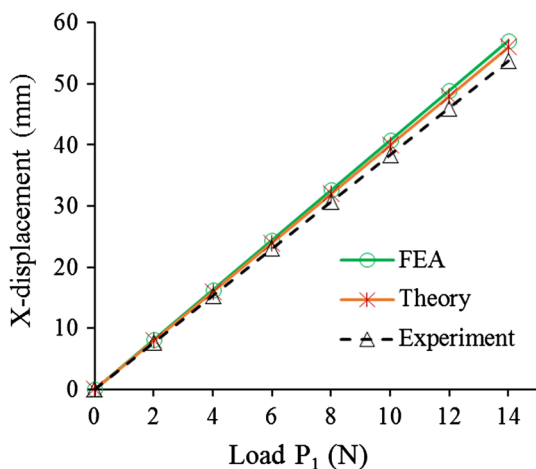


Fig. 10 Bending  $x$ -displacement versus load  $P_1$

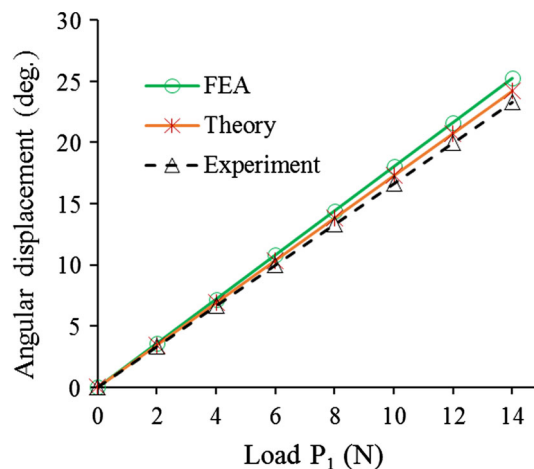


Fig. 11 Angular displacement versus load  $P_1$

bending displacement of the joint along the  $x$ -axis, a force gauge (Lutron, tension and compression, maximum 196 N, DC 9 V adapter, Model: NF-9500, Taiwan) was employed to give the force. A digital indicator (high precision 0.001 mm IPC ID-C112, Mitutoyo, Japan) was utilized to realize the displacement of the BICJ, as given in Fig. 9b. The axial displacement along the  $y$ -axis was measured, as illustrated in Fig. 9c. The rotational angle of the joint was measured, as shown in Fig. 9d by using a force gauge (model AK-2, ALGOL Instrument Co., LTD, Taiwan) to give the load and digital indicator. The experimentations were repeated six times to get the average value.

In order to compare the analytical model with simulation and experiments, the displacement of the proposed BICJ along the  $x$ -axis was computed. The load  $P_1$  from 2 to 14 N exerted to the free end of prototype, and the corresponding bending deflection was recorded. Besides, the FEA simulation in ANSYS 18.1 software was carried out so as to get the simulated displacement. As shown in Fig. 10, the results revealed that the deviation error between the analytical model and FEA simulation is about 1.88%. The error between the analytical model and experiments is approximately 4.16%. These errors are relatively small, and it validates the accuracy of analytical model.

Under the load  $P_1$ , the angular displacement/rotational angle was calculated; the simulation and experiments were performed. As seen in Fig. 11, the results found that the error between analytical model and simulation is about 4.34%. The error between analytical model and experiment is 8.46%. Similarly, the compressive displacements were recorded and compared with simulation and experiments, as seen in Fig. 12. The results showed that the error between the theory and simulation is about 4.6% and the error between the theory and experiment is approximately 6.38%.

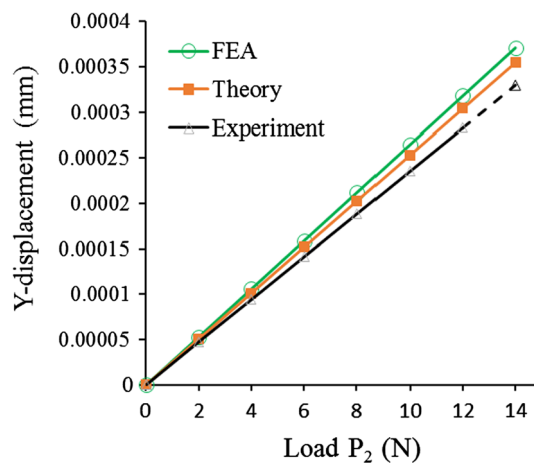


Fig. 12 Compressive displacement versus load  $P_2$

### 5.2 Improvement of Performances

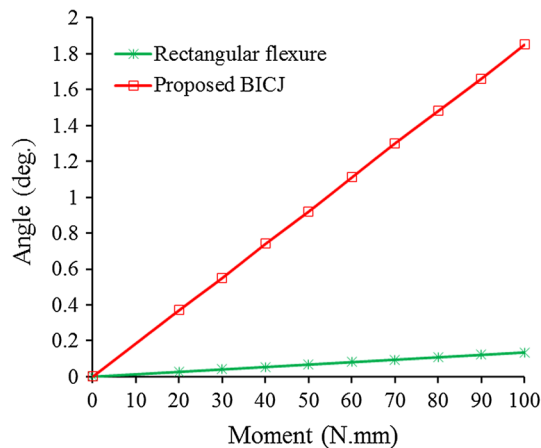
The effectiveness of the proposed BICJ was compared with the rectangular cross section flexure. The dimensions of flexure included in-of-plane thickness of 4 mm, length of 88 mm, and out-of-plane width of 10 mm. Under load  $P_1$  and the use of Eq. (10), the results showed that an increase in bending displacement of the proposed BICJ is about 14.6%, as shown in Table 10. Using Eq. (11), the results found that an increase in angular displacement of the proposed BICJ is approximately 12.6%, as given in Table 10. Besides, the flexibility and compliance of the proposed joint are better than those of rectangular flexure.

Using Eq. (12) and FEA simulation, the relation of moment load versus rotation angle is described in Fig. 13. Under a moment load from 0 to 100 N mm, it found that the rotation angle of the proposed BICJ is much larger than that of the rectangular flexure.



**Table 10** Increased performances: bending displacement and angular displacement

$P_1$ (N)	2	4	6	8	10	12	14
Bending displacement ( $I_b$ )							
Increase (%)	14.6782	14.6791	14.6783	14.6779	14.6782	14.6783	14.6781
Angular displacement ( $I_a$ )							
Increase (%)	12.6714	12.6718	12.6721	12.6716	12.6719	12.6713	12.6721

**Fig. 13** Rotational angle versus moment

## 6 Conclusions

This paper has presented design and analysis for a new butterfly-inspired compliant joint. By adopting the foldable mechanism and butterfly's profile, the BICJ's equivalent spring stiffness was varied easily. The conceptual design of the proposed BICJ was presented. The performances of the BICJ were validated by comparing with the joints #33 and #X through FEA simulation. The results showed that the performances of BICJ outperform other joints.

The closed-form model of the BICJ was provided, and the equations for calculating the stiffness, displacement, and rotation angle for the proposed joint were derived. Compared with a conventional rectangular flexure joint, the BICJ showed a great improvement. Specifically, the results indicated that an increase in bending displacement of proposed BICJ is about 14.6%, and an increase in angular displacement of proposed BICJ is approximately 12.6% in comparison with the rectangular flexure joint.

The results showed that there is a good agreement between the analytical model, simulation, and experimental results. These results well coincided with each other that confirmed the closed-form model. Finally, the proposed BICJ joint can be a promising candidate for different positioning applications. The results of this article may open possibilities for studying a new class of compliant joints with multiple functions in future work.

**Acknowledgements** This research is funded by Vietnam National Foundation for Science and Technology Development (NAFOSTED) under Grant No. 107.01-2019.14.

## Compliance with Ethical Standards

**Conflict of interest** The authors declare that they have no conflict of interest.

## References

- Du, Z.; Yang, M.; Dong, W.; Zhang, D.: Static deformation modeling and analysis of flexure hinges made of a shape memory alloy. *Smart Mater. Struct.* **25**, 115029 (2016). <https://doi.org/10.1088/0964-1726/25/11/115029>
- Le Chau, N.; Le, H.G.; Dao, T.-P.; Dang, V.A.: Design and optimization for a new compliant planar spring of upper limb assistive device using hybrid approach of RSM-FEM and MOGA. *Arab. J. Sci. Eng.* **44**, 7441–7456 (2019). <https://doi.org/10.1007/s13369-019-03795-w>
- Liu, L.; Bi, S.; Yang, Q.; Wang, Y.: Design and experiment of generalized triple-cross-spring flexure pivots applied to the ultra-precision instruments. *Rev. Sci. Instrum.* **85**, 105102 (2014)
- Jones, J.A.; Lee, Y.; Moore, J.Z.: Parametric study for asymmetric flexure hinge design for tissue cutting. *Proc. Inst. Mech. Eng. B J. Eng. Manuf.* **233**, 1302–1309 (2018). <https://doi.org/10.1177/0954405418774587>
- Liang, C.; Wang, F.; Tian, Y.; Zhao, X.; Zhang, H.: A novel monolithic piezoelectric actuated flexure-mechanism based wire clamp for microelectronic device packaging. *Rev. Sci. Instrum.* **86**, 045106 (2015)
- Dao, T.-P.; Huang, S.-C.: Optimization of a two degrees of freedom compliant mechanism using Taguchi method-based grey relational analysis. *Microsyst. Technol.* **23**, 4815–4830 (2017). <https://doi.org/10.1007/s00542-017-3292-1>
- Dao, T.-P.; Huang, S.-C.: Design and analysis of a compliant micro-positioning platform with embedded strain gauges and viscoelastic damper. *Microsyst. Technol.* **23**, 441–456 (2017). <https://doi.org/10.1007/s00542-016-3048-3>
- Sun, X.; Yang, B.: A new methodology for developing flexure-hinged displacement amplifiers with micro-vibration suppression for a giant magnetostrictive micro drive system. *Sens. Actuators A Phys.* **263**, 30–43 (2017). <https://doi.org/10.1016/j.sna.2017.04.009>
- Wang, X.; Liu, C.; Gu, J.; Zhang, W.: A parametric model for rotational compliance of a cracked right circular flexure hinge. *Int. J. Mech. Sci.* **94–95**, 168–173 (2015). <https://doi.org/10.1016/j.ijmecsci.2015.02.012>
- Chen, G.; Ma, Y.; Li, J.: A tensural displacement amplifier employing elliptic-arc flexure hinges. *Sens. Actuators A Phys.* **247**, 307–315 (2016). <https://doi.org/10.1016/j.sna.2016.05.015>

11. Chen, Z.; Chen, G.; Zhang, X.: Damped leaf flexure hinge. *Rev. Sci. Instrum.* **86**, 055002 (2015)
12. Valentini, P.P.; Cirelli, M.; Pennestrì, E.: Second-order approximation pseudo-rigid model of flexure hinge with parabolic variable thickness. *Mech. Mach. Theory* **136**, 178–189 (2019). <https://doi.org/10.1016/j.mechmachtheory.2019.03.006>
13. Chau, N.L.; et al.: Efficient hybrid method of FEA-based RSM and PSO algorithm for multi-objective optimization design for a compliant rotary joint for upper limb assistive device. *Math. Probl. Eng.* **2019**, 1–14 (2019)
14. Nguyen, D.N.; et al.: Hybrid approach of finite element method, Kriging metamodel, and multiobjective genetic algorithm for computational optimization of a flexure elbow joint for upper-limb assistive device. *Complexity* **2019**, 1–13 (2019)
15. Ding, B.; Yang, Z.X.; Xiao, X.; Zhang, G.: Design of reconfigurable planar micro-positioning stages based on function modules. *IEEE Access* **7**, 15102–15112 (2019). <https://doi.org/10.1109/ACCESS.2019.2894619>
16. Chen, Z.; Jiang, X.; Zhang, X.: Damped circular hinge with integrated comb-like substructures ☆. *Precis. Eng.* **53**, 212–220 (2018). <https://doi.org/10.1016/j.precisioneng.2018.04.004>
17. Qiang, L.; Cunyun, P.; Xiaojun, X.: Closed-form compliance equations for power-function-shaped flexure hinge based on unit-load method. *Precis. Eng.* **37**, 135–145 (2013). <https://doi.org/10.1016/j.precisioneng.2012.07.010>
18. Lee, V.D.; Gibert, J.M.; Ziegert, J.C.: Hybrid bi-directional flexure joint ☆. *Precis. Eng.* **38**, 270–278 (2014). <https://doi.org/10.1016/j.precisioneng.2013.10.001>
19. Li, L.; Zhang, D.; Guo, S.; Qu, H.: Design, modeling, and analysis of hybrid flexure hinges. *Mach. Theory* **131**, 300–316 (2019). <https://doi.org/10.1016/j.mechmachtheory.2018.10.005>
20. Lobontiu, N.; Wight-crask, J.; Kawagley, C.: Straight-axis folded flexure hinges: in-plane elastic response. *Precis. Eng.* **57**, 54–63 (2019). <https://doi.org/10.1016/j.precisioneng.2019.03.006>
21. Qiu, L.; Yue, X.; Xie, Z.: Design and analysis of multicavity flexure hinge (MCFH) based on three-dimensional continuum topology optimization. *Mech. Mach. Theory* **139**, 21–33 (2019). <https://doi.org/10.1016/j.mechmachtheory.2019.04.004>
22. Hopkins, J.B.; Culppepper, M.L.: Synthesis of precision serial flexure systems using freedom and constraint topologies (FACT). *Precis. Eng.* **35**, 638–649 (2011). <https://doi.org/10.1016/j.precisioneng.2011.04.006>
23. Friedrich, R.; Lammering, R.; Rösner, M.: On the modeling of flexure hinge mechanisms with finite beam elements of variable cross section. *Precis. Eng.* **38**, 915–920 (2014). <https://doi.org/10.1016/j.precisioneng.2014.06.001>
24. Merriam, E.G.; Lund, J.M.; Howell, L.L.: Compound joints: behavior and benefits of flexure arrays. *Precis. Eng.* **45**, 79–89 (2016). <https://doi.org/10.1016/j.precisioneng.2016.01.011>
25. Merriam, E.G.; Howell, L.L.: Non-dimensional approach for static balancing of rotational flexures. *MAMT* **84**, 90–98 (2015). <https://doi.org/10.1016/j.mechmachtheory.2014.10.006>
26. Moon, Y.-M.; Trease, B.P.; Kota, S.: Design of large-displacement compliant joints. In: *ASME 2002 International Design Engineering Technical Conferences and Computers and Information in Engineering Conference*. American Society of Mechanical Engineers Digital Collection (2002)
27. Liu, M.; Zhang, X.; Fatikow, S.: Design of flexure hinges based on stress-constrained topology optimization. *Proc. Inst. Mech. Eng. C J. Mech. Eng. Sci.* **231**, 4635–4645 (2016). <https://doi.org/10.1177/0954406216671346>
28. Lu, Q.; Cui, Z.; Chen, X.; Lu, Q.; Cui, Z.; Chen, X.: Fuzzy multi-objective optimization for movement performance of deep-notch elliptical flexure hinges. *Rev. Sci. Instrum.* **86**, 065005 (2015). <https://doi.org/10.1063/1.4922914>
29. Le Chau, N.; Dang, V.A.; Le, H.G.; Dao, T.-P.: Robust parameter design and analysis of a leaf compliant joint for micropositioning systems. *Arab. J. Sci. Eng.* **42**, 4811–4823 (2017). <https://doi.org/10.1007/s13369-017-2682-0>
30. Yang, H.; Liu, R.; Wang, Y.; Deng, Z.: Experiment and multiobjective optimization design of tape-spring hinges. *Struct. Multidiscip. Optim.* **51**, 1373–1384 (2014). <https://doi.org/10.1007/s00158-014-1205-9>
31. Wang, R.; Zhou, X.; Zhu, Z.; Liu, Q.: Development of a novel type of hybrid non-symmetric flexure hinges. *Rev. Sci. Instrum.* **86**, 085003 (2015). <https://doi.org/10.1063/1.4928593>
32. Valentini, P.P.; Pennestrì, E.: Elasto-kinematic comparison of flexure hinges undergoing large displacement. *Mech. Mach. Theory* **110**, 50–60 (2017). <https://doi.org/10.1016/j.mechmachtheory.2016.12.006>
33. Zheng, X.; Wei, F.; Chen, H.; Guo, S.; Xuan, F.: Measurement of small rotation angle of flange joints by a novel flexure. *Measurement* **145**, 244–253 (2019). <https://doi.org/10.1016/j.measurement.2019.05.090>
34. Ma, J.; Huang, X.; Bae, H.; Zheng, Y.; Zhao, M.; Yu, M.: Liquid viscosity measurement using a vibrating flexure hinged structure and a fiber optic sensor. *IEEE Sens. J.* **16**, 5249–5258 (2016). <https://doi.org/10.1109/JSEN.2016.2562740>
35. Dao, T.P.; Huang, S.C.: Compliant thin-walled joint based on zygoptera nonlinear geometry. *J. Mech. Sci. Technol.* **31**, 1293–1303 (2017). <https://doi.org/10.1007/s12206-017-0228-8>
36. Le Chau, N.; Dao, T.P.; Nguyen, V.T.T.: Optimal design of a dragonfly-inspired compliant joint for camera positioning system of nanoindentation tester based on a hybrid integration of Jaya-ANFIS. *Math. Probl. Eng.* (2018). <https://doi.org/10.1155/2018/8546095>
37. Pei, X.; Yu, J.; Zong, G.; Bi, S.: A family of butterfly flexural joints: Q-lift pivots. *J. Mech. Des.* (2016). <https://doi.org/10.1115/1.4007917>
38. Ho, N.L.; Dao, T.P.; Le Chau, N.; Huang, S.C.: Multi-objective optimization design of a compliant microgripper based on hybrid teaching learning-based optimization algorithm. *Microsyst. Technol.* **6**, 1–17 (2018). <https://doi.org/10.1007/s00542-018-4222-6>
39. Choi, K.; Lee, J.J.; Kim, G.H.; Lim, H.J.; Kwon, S.G.: Amplification ratio analysis of a bridge-type mechanical amplification mechanism based on a fully compliant model. *Mech. Mach. Theory* **121**, 355–372 (2018). <https://doi.org/10.1016/j.mechmachtheory.2017.11.002>
40. Phung, M.; Hieu, D.; Le, G.; Le, N.; Thanh, C.; Dao, P.: A multi-objective optimization design for a new linear compliant mechanism. Springer, New York (2019)

